
SCALING AND FINITE-SIZE EFFECTS FOR THE CRITICAL BACKBONE

M. BARTHELEMY,* S. V. BULDYREV,* S. HAVLIN,[†] and H. E. STANLEY*

**Center for Polymer Studies, Boston University,
Boston, 02215 MA, USA*

*[†]Minerva Center and Department of Physics, Bar-Ilan University,
Ramat-Gan 52900, Israel*

Abstract

In a first part, we study the backbone connecting two given sites of a two-dimensional lattice separated by an arbitrary distance r in a system of size L . We find a scaling form for the average backbone mass and we also propose a scaling form for the probability distribution $P(M_B)$ of backbone mass for a given r . For $r \approx L$, $P(M_B)$ is peaked around L^{d_B} , whereas for $r \ll L$, $P(M_B)$ decreases as a power law, $M_B^{-\tau_B}$, with $\tau_B \simeq 1.20 \pm 0.03$. The exponents ψ and τ_B satisfy the relation $\psi = d_B(\tau_B - 1)$, and ψ is the codimension of the backbone, $\psi = d - d_B$. In a second part, we study the multifractal spectrum of the current in the two-dimensional random resistor network at the percolation threshold. Our numerical results suggest that in the infinite system limit, the probability distribution behaves for small i as $P(i) \sim 1/i$ where i is the current. As a consequence, the moments of i of order $q \leq q_c = 0$ diverge with system size, and all sets of bonds with current values below the most probable one have the fractal dimension of the backbone. Hence we hypothesize that the backbone can be described in terms of only (i) blobs of fractal dimension d_B and (ii) high current carrying bonds of fractal dimension going from d_{red} to d_B , where d_{red} is the fractal dimension of the red bonds carrying the maximal current.

1. SCALING FOR THE CRITICAL BACKBONE

The percolation problem is a classical model of phase transitions, as well as a useful model for describing connectivity phenomena, and in particular for describing porous media.¹⁻³ At the percolation threshold p_c , the mass of the largest cluster scales with the system size L

as $M \sim L^{d_f}$. The fractal dimension d_f is related to the space dimension d and to the order parameter and correlation length exponents β and ν by $d_f = d - \beta/\nu$.¹⁻³ In two dimensions, $d_f = 91/48$ is known exactly.

An interesting subset of the percolation cluster is the backbone which is obtained by removing the non-current carrying bonds from the percolation cluster.⁴ The structure of the backbone consists of blobs and links.^{1,5-7} The backbone can in fact be further partitioned into subsets according to the magnitude of the electric current carried.^{8,9} The backbone is relevant to transport properties¹⁻³ and fracture.¹⁰ The fractal dimension d_B of the backbone can be defined via its typical mass M_B , which scales with the system size L as $M_B \sim L^{d_B}$. The backbone dimension is an independent exponent and its exact value is not known. A current numerical estimate¹¹ is $d_B = 1.6432 \pm 0.0008$.

The operational definition of the backbone has an interesting history.¹⁻³ Customarily, one defines the backbone using parallel bars, and looks for the percolation cluster (and the backbone) which connects the two sides of the system.⁴ A different situation arises in oil field applications,¹² where one studies the backbone connecting two wells separated by an *arbitrary* distance r . This situation is important for transport properties, since in oil recovery one injects water at one point and recovers oil at another point.¹² From a fundamental point of view, it is important to understand how the percolation properties depend on different boundary conditions.

We study in this first part the backbone connecting two points separated by an arbitrary distance r in a two-dimensional system of linear size L . One goal¹³ is to understand the distribution of the backbone mass $M_B(r, L)$, and how its average value scales with r and L in the entire range $0 < r < L$.

We choose two sites A and B belonging to the infinite percolating cluster on a two-dimensional square lattice (the fraction of bonds is $p = p_c = 1/2$). A and B are separated by a distance r and symmetrically located between the boundaries.¹⁴ Using the burning algorithm, we determine the backbone connecting these two points for values of L ranging from 100 to 1000. For each value of L , we consider a sequence of values of r with $2 \leq r \leq L - 2$. In order to test the universality of the exponents, we perform our study on three lattices: square, honeycomb and triangular lattice. For simplicity, we restrict our discussion here to the square lattice, as we find similar results for the other two lattices.

We begin by studying the backbone mass probability distribution $P(M_B)$. We show that $P(M_B)$ obeys a simple scaling form in the entire range of r/L ,

$$P(M_B) \sim \frac{1}{r^{d_B}} F\left(\frac{M_B}{r^{d_B}}\right), \quad (1)$$

where $F(x)$ is a scaling function, whose shape depends on the ratio r/L .

For $r \approx L$, it seems reasonable to assume that $P(M_B)$ will be peaked around its average value $\langle M_B \rangle \sim L^{d_B}$. The data collapse predicted by Eq. (1) is represented in Fig. 1. In this case, the scaling function F is peaked at approximately L^{d_B} . However, the case $r \ll L$ is far less clear. In fact, we expect for $r \ll L$ that the backbone mass fluctuates greatly from one realization to another, since its minimum value can be r and its maximum can be of order L^{d_f} . $P(M_B)$ has a lower cut-off of order r (since the backbone must connect points A and B) and an upper cut-off of order L^{d_B} . We find good data collapse (Fig. 2), which indicates that the scaling function F is a power law in the range from r^{d_B} to L^{d_B} , with exponent approximately $\tau_B \simeq 1.20 \pm 0.03$ (there is a cut-off at $M_B \sim L^{d_B}$ not shown here). The exponent τ_B is connected to the blob size distribution⁵ since typically, the two sites

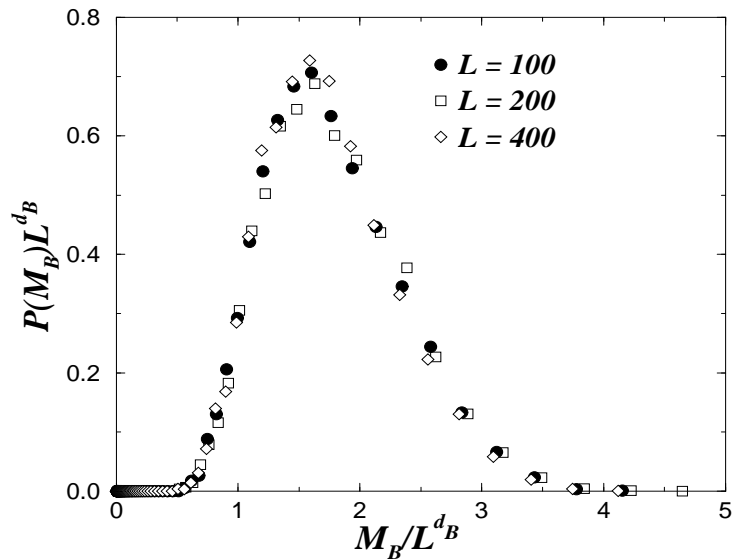


Fig. 1 Rescaled backbone mass distribution in the case $r \ll L$.

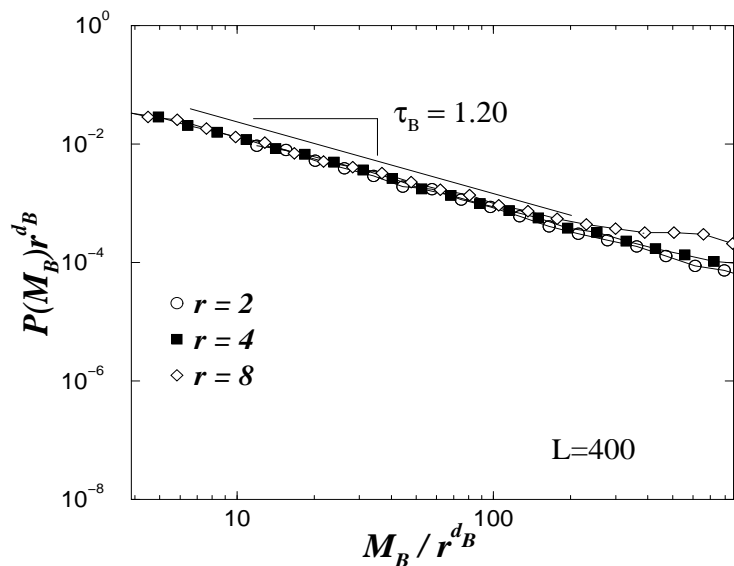


Fig. 2 Rescaled backbone mass distribution in the case $r \simeq L$.

belong to the same blob, and the sampling of backbones is equivalent to sampling of the blobs. From,⁵

$$\frac{d}{d_B} = \tau_B. \quad (2)$$

This relation gives the estimate $\tau_B \simeq 1.22$ in good agreement with our numerical simulation.

We now study the average backbone mass $\langle M_B \rangle$. From dimensional considerations, the r dependence can only be a function of r/L . We thus propose the following *Ansatz*:

$$\langle M_B(r, L) \rangle = L^{d_B} G\left(\frac{r}{L}\right). \quad (3)$$

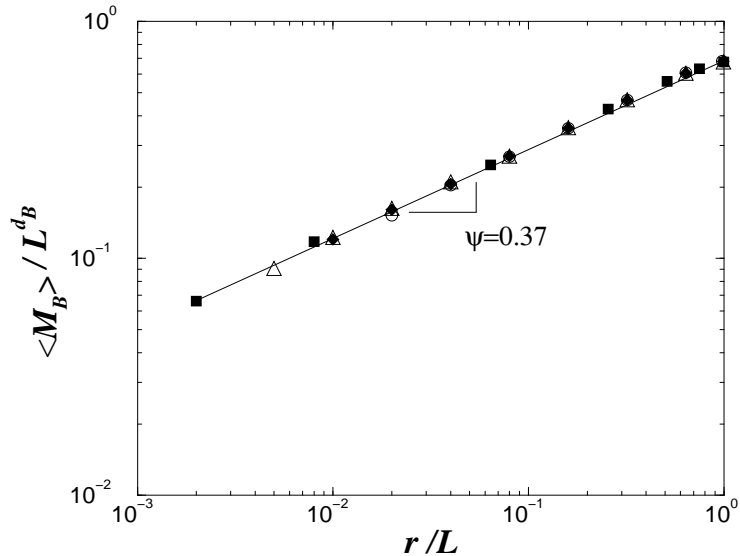


Fig. 3 Rescaled average backbone mass versus versus r/L .

In order to test the Eq. (3), we scale the data of M_B versus r for different values of L . The data collapse is obtained using $d_B = 1.65$ and is shown on Fig. 3. This (log-log) plot supports the scaling Ansatz (3). Moreover, one can see that the scaling function G is, surprisingly, a pure power law on the entire range $[0, 1]$, with exponent $\psi = 0.37 \pm 0.02$. The results (1) and (3) are consistent, since if (1) holds with a power law behavior for the scaling function $F(x) \sim x^{-\tau_B}$ for $x > 1$, and $F(x) = 0$ for $x < 1$, then the average mass is given by

$$\langle M_B(r, L) \rangle = \int_r^{L^{d_B}} F\left(\frac{M}{r^{d_B}}\right) \frac{dM}{r^{d_B}} M. \quad (4)$$

Assuming that L/r is large enough, the integral in (4) can be approximated as $L^{d_B - \psi} r^\psi$, where

$$\psi = d_B(\tau_B - 1). \quad (5)$$

In our simulation $\tau_B \approx 1.20 \pm 0.03$, which leads to the value $\psi \approx 0.33 \pm 0.05$ in reasonable agreement with the value measured directly on the average mass.

Moreover, using Eq. (2) together with Eq. (5), we obtain

$$\psi = d - d_B \quad (6)$$

which means that ψ is the codimension of the fractal backbone.

To summarize, we find that for any value of r/L , the scaling form, Eq. (1), for the probability distribution is valid. The shape of the scaling function F depends on r/L , being a peaked distribution for $r \approx L$, and a power law for $r \ll L$. The average backbone mass varies with r and L according to Eq. (4). For fixed system size, it varies as $\langle M_B \rangle \simeq r^\psi$ (for $0 < r < L$). The value of ψ is small ($\psi \approx 0.37$) indicating that the backbone mass does not change drastically as r changes. On the other hand, the exponent governing the variation of $\langle M_B \rangle$ with L for fixed r is expected to be larger, with $\langle M_B \rangle \sim r^{d_B - \psi}$. This exponent $d_B - \psi$ is not equal to the fractal dimension d_B of the backbone, but is smaller by an amount equal to ψ .

2. MULTIFRACTAL SPECTRUM AND FINITE-SIZE EFFECTS

The transport properties of the percolating cluster have been the subject of numerous studies during the last twenty years.^{2,15} A particularly interesting system is the random resistor network (RRN), where the bonds have a random conductance. The random resistor network serves as a paradigm for many transport properties in heterogeneous systems as well as being a simplified model for fracture.¹⁰

The first studies of the RRN were devoted to effective properties of the network (conductivity, permittivity, etc.),^{16,17} but for many practical applications — such as fracture, and dielectric breakdown¹⁰ — the central quantity is the probability distribution $P(i)$ of currents i . For instance, in the random fuse network, it is the maximum current corresponding the hottest or “red” bonds which will determine the macroscopic failure of the system.¹⁰

The probability distribution $P(i)$ has many interesting features, one of which is multifractality:^{9,18–20} in order to describe $P(i)$, an infinite set of exponents is needed. This idea of multifractality was initially proposed to treat turbulence²¹ and later applied successfully in many different fields, ranging from model systems such as DLA²² to physiological data such as heartbeat.²³

It was first believed^{9,20} that the low current part of $P(i)$ and of the multifractal spectrum follow a log-normal law as it is the case on hierarchical lattices. It is now clear,²⁵ that for small currents, the current probability distribution follows a power law $P(i) \sim i^{b-1}$ where $b \geq 0$. For large currents, the distribution quickly converges to an infinite system limit with no dependence on the system size L . For small currents, governed by very long paths, the distribution converges more slowly. It was suggested^{24,25} that the exponent b of the low-current part has a $1/\log L$ dependence. The asymptotic value b_∞ of the exponent b for the infinite system is of crucial importance. If b_∞ is finite and positive, then a subset of bonds with low current has a fractal dimension depending on its value. On the other hand, if b_∞ is zero, then the low current part of the multifractal spectrum is flat, and the subset of bonds with any low value of current has the same fractal dimension as the entire backbone. It is thus important to understand if the apparent subset structure with different fractal dimensions arises primarily from finite-size effects.

Previous estimates of b_∞ include $b_\infty = 0$ ²⁴ and $b_\infty \gtrsim 0.25$,²⁵ but the maximum value of L used was 128.²⁴ In this part, we study a sequence of sizes from $L = 50$ to $L = 1000$, and hypothesize²⁶ that $b_\infty = 0$.

We first recall the basis of multifractality applied to the percolating two-dimensional resistor network of linear size L . Let $n(i, L)$ be the number of bonds carrying current i . For large L , $n(i, L)$ scales as^{9,20}

$$n(i, L) \sim L^{f(\alpha, L)} \quad (7)$$

where $\alpha \equiv -\log i / \log L$. The multifractal spectrum $f(\alpha, L) \equiv \log n / \log L$ can thus be interpreted as the fractal dimension of the subset of bonds carrying the current i . The q -th moment of the current is defined as $M_q \equiv \langle \sum i^q \rangle$, where the sum is over all bonds carrying a non-zero current and $\langle \dots \rangle$ denotes an average over different disorder configurations. These moments exists for $q > q_c$, and it can be easily shown²⁵ that the “threshold” is $q_c = -b$. The asymptotic slope thus give the asymptotic value of the threshold q_c .

For the fixed current ensemble, one finds $M_q \sim L^{\tau_q}$ for large L and for $q > q_c$ and where τ_q is an exponent that depends on q .^{9,20} In particular, $\tau_0 = d_B$, $\tau_2 = t/\nu$, and $\tau_\infty = 1/\nu$ ²⁸ where d_B is the fractal dimension of the backbone, t the conductivity exponent, and ν is the correlation length exponent. If the behavior is monofractal, then τ_q is a linear function

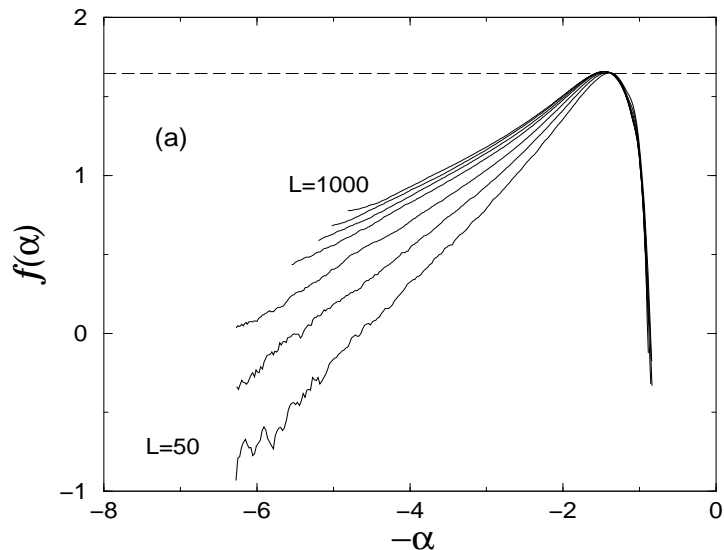


Fig. 4 Multifractal spectrum for $r \simeq L$ going from 50 to 1000.

of q with the intercept equal to the fractal dimension of the monofractal, while in the multifractal case, the exponents are not described by a simple linear function of q . In the $L \rightarrow \infty$ limit, knowing $f(\alpha)$ is equivalent to knowing the infinite set of exponents τ_q , as $f(\alpha) = \tau_q - qd\tau/dq$ is the Legendre transform of τ_q .¹⁰

The low current part of $f(\alpha, L)$ was found numerically to be a power law of slope $b = b(L)$. It was suggested that

$$b(L) = b_\infty + \frac{a}{\log L} + \dots \quad (8)$$

which is a strong finite-size effect since $\log L$ grows very slowly, and two possibilities for b_∞ were proposed, $b_\infty = 0$ ²⁴ or $b_\infty = 1/4$.²⁵

We consider the two-dimensional random resistor network at criticality, i.e. the fraction of conducting bonds p is equal to its critical value $p = p_c = 1/2$. We first apply a voltage difference between two parallel bars. We compute $f(\alpha, L)$, for a fixed voltage difference, for $L = 50, \dots, 1000$, and average over 10^4 configurations for each L . We show our results in Fig. 4. The slope b is clearly decreasing with L , confirming the strong finite size effects already observed.^{24,25} Next, we consider a second type of configuration, which we call the “two injection points” case, in contrast with the usual “parallel bars” case. We impose a voltage difference between two points A and B separated by a distance r , and we look for the backbone connecting these two points. This situation was studied in,^{13,27} but here we keep only the backbones of linear size L . In this way, we have large backbones connecting the two points A and B , and for $r \ll L$ we expect to have a large number of small currents on bonds belonging to long loops. The multifractal spectrum is then defined in the same way as for the parallel bars and we calculate the slope of the small current part of the multifractal spectrum for different values of L . The variation of the slope for the two-injection-points case is shown in Fig. 5. We observe that there is a large amount of small currents, and that the asymptotic limit is reached faster in this case. We expect that the low current distribution will be asymptotically the same as in the parallel bar case, so the consistency between the two configurations supports our results. For large currents there are some distinct differences in the multifractal spectrum.²⁹

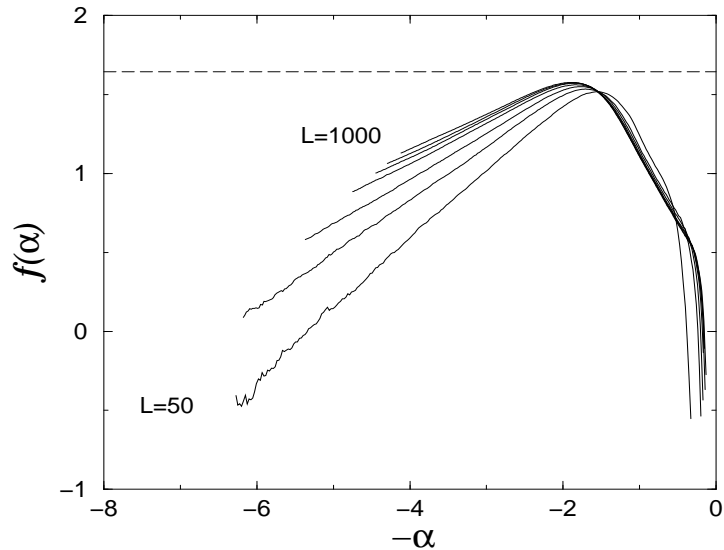


Fig. 5 Multifractal spectrum for $r = 4 \ll L$ and L is going from 50 to 1000.

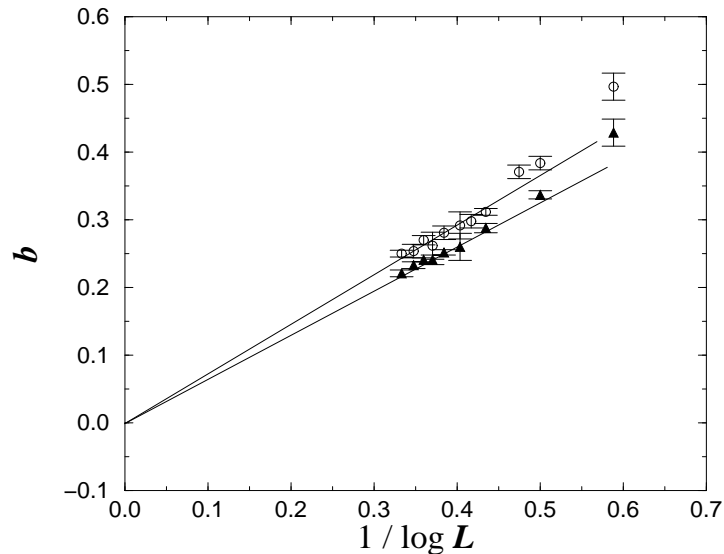


Fig. 6 Slope b versus $1/\log L$. The circles correspond to the parallel bars and the triangles to the ‘two-injection’ case.

Figure 6 shows the slope b versus $1/\log L$ according to Eq. (8) for both multifractal spectra. The extrapolation to $L = \infty$ is consistent with $b_\infty = 0$ in both cases. This result is consistent with the behavior of the successive intercepts (Fig. 7). Another functional form of b versus L could lead to another value of b_∞ . If we replace the abscissa of Figs. 2(a) and (b) by $1/(\log L)^\alpha$, then we find that the extrapolated value for b_∞ depends on α , ranging from $b_\infty \simeq 0.10$ for $\alpha = 2$ to $b_\infty < 0$ (which is impossible) for $\alpha = 0.5$. It is numerically difficult to distinguish between a $1/\log L$ and a $1/(\log L)^2$ behavior, but the $1/\log L$ is the most commonly used.^{24,25} If we accept this functional form, then our results are consistent with $b_\infty = 0$. Finally, we note that the sequence of maximum values of $f(\alpha, L)$ for the two injection points case plausibly extrapolates in the variable $1/\log L$ as $L \rightarrow \infty$ to a value of d_B close to the known value 1.64.

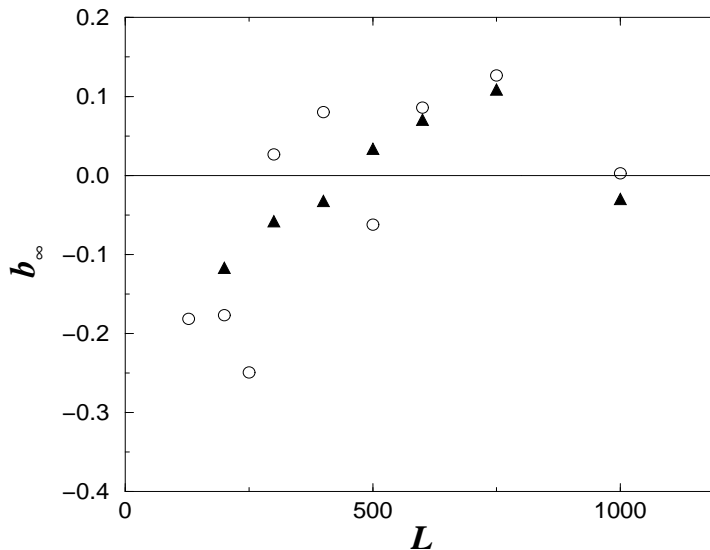


Fig. 7 Successive intercepts computed from the datas of Fig. 6.

Thus our results suggest the intriguing possibility that for $L \rightarrow \infty$, the small current part of $f(\alpha, L)$ is a horizontal line at the value d_B , implying that in an infinite system the fractal dimension of the subset contributing to small current is d_B , independently of the value of i . In this sense, the small current probability distribution is apparently not multifractal. The “perfectly balanced” bonds which carry zero current have a fractal dimension equal to d_B .²⁴ Since these bonds contribute to $f(\alpha)$ for $\alpha \rightarrow \infty$, the fact that their fractal dimension is d_B supports our hypothesis that $b_\infty = 0$. A related conclusion is that $q_c = 0$ or, in other words, the negative moments of the current diverge in the infinite-size limit. In particular, it shows that the first-passage time for a tracer particle travelling in a flow field in a porous medium modelled by a percolation cluster diverges in an infinite system.

For large values of the current, the multifractal features are stable against L increase. This suggests that in the infinite-size limit, there are essentially two different type of subsets; the first comprises the blobs of fractal dimension d_B , and the second set comprises links carrying larger values of the current (including red bonds, which carry all the current), of fractal dimension ranging from $d_{\text{red}} = 1/\nu$ to d_B .

ACKNOWLEDGMENTS

We thank L. A. N. Amaral for valuable help and A. Chessa, A. Coniglio, N. V. Dokholyan, P. Gopikrishnan, P. R. King, G. Paul, A. Scala, and F. W. Starr for useful discussions. We thank especially J. S. Andrade for providing the software for finding currents, and DGA and NSF for financial support.

REFERENCES

1. A. Bunde and S. Havlin (eds.), *Fractals and Disordered Systems*, 2nd ed. (Springer, Berlin, 1996), and refs. therein.
2. D. Stauffer and A. Aharony, *Introduction to Percolation Theory* (Taylor and Francis, London, 1992).
3. M. Sahimi, *Applications of Percolation Theory* (Taylor and Francis, London, 1992).

4. S. Kirkpatrick, *AIP Conf. Proc.* **40**, 99 (1978); G. Shlifer, W. Klein, P. J. Reynolds and H. E. Stanley, *J. Phys.* **A12**, L169 (1979).
5. H. J. Herrmann and H. E. Stanley, *Phys. Rev. Lett.* **53**, 1121 (1984).
6. H. E. Stanley, *J. Phys.* **A10**, L211 (1977).
7. A. Coniglio, *Phys. Rev. Lett.* **46**, 250 (1981).
8. R. Rammal, C. Tannous, P. Breton and A. M. S. Tremblay, *Phys. Rev. Lett* **54**, 1718 (1985).
9. L. de Arcangelis, A. Coniglio and S. Redner, *Phys. Rev.* **B36**, 5631 (1987).
10. H. Herrmann and S. Roux (eds.), *Statistical Models for the Fracture of Disordered Media* (North-Holland, 1990).
11. P. Grassberger, *Physica* **A262**, 251 (1999).
12. Y. Lee, J. S. Andrade Jr, S. V. Buldyrev, S. Havlin, P. R. King, G. Paul and H. E. Stanley, *preprint Cond-Mat 9903066*.
13. M. Barthélémy, S. V. Buldyrev, S. Havlin and H. E. Stanley, *Phys. Rev.* **E60**, R1123 (1999).
14. H. J. Herrmann, D. Hong and H. E. Stanley, *J. Phys.* **A17**, L261 (1984).
15. A. Coniglio and M. Zannetti, *Physica* **D38**, 37 (1989).
16. R. Landauer, in *Proceedings of the 1st Conference on Electrical and Optical Properties of Inhomogeneous Media* (Ohio State University, 1977), *AIP Conf. Proc. No. 40*, eds. J. C. Garland and D. B. Tanner (AIP, New York, 1978).
17. D. J. Bergman and D. Stroud, *Solid State Physics* **46**, 147 (1992).
18. R. Rammal, C. Tannous and A.-M. S. Tremblay, *Phys. Rev.* **A31**, 2662 (1985).
19. R. Rammal, C. Tannous, P. Breton and A.-M. S. Tremblay, *Phys. Rev. Lett.* **54**, 1718 (1985).
20. L. de Arcangelis, S. Redner and A. Coniglio, *Phys. Rev.* **B34**, 4656 (1986).
21. B. B. Mandelbrot, *J. Fluid Mech.* **62**, 331 (1974).
22. See, e.g., J. Lee et al., *Phys. Rev.* **A39**, 6545 (1989).
23. P. Ch. Ivanov et al., *Nature* **399**, 461 (1999).
24. G. Batrouni, A. Hansen and S. Roux, *Phys. Rev.* **A38**, 3820 (1988).
25. A. Aharony, R. Blumenfeld and A. B. Harris, *Phys. Rev.* **B47**, 5756 (1993).
26. M. Barthélémy, S. V. Buldyrev, S. Havlin and H. E. Stanley, *Phys. Rev.* **E61**, R3283 (2000).
27. Y. Lee et al., *Phys. Rev.* **E60**, 3425 (1999).
28. A. Coniglio, *J. Phys.* **A15**, 3829 (1982).
29. In the “two injection points” configuration, the large currents are controlled by the small loops between A and B . The fluctuation of the length of the shortest path between A and B gives thus rise to the region of power law behavior for large currents we observe in Fig. 5.
30. G. Batrouni, A. Hansen and B. Larson, *Phys. Rev.* **B53**, 2292 (1998).
31. H. E. Daniels, *Ann. Math. Stat.* **25**, 631 (1954).
32. B. B. Mandelbrot and C. J. G. Evertsz, *Physica* **A168**, 95 (1990).
33. B. B. Mandelbrot, C. J. G. Evertsz and Y. Hayakawa, *Phys. Rev.* **B42**, 4528 (1990).